We are IntechOpen, the world's leading publisher of Open Access books Built by scientists, for scientists

6,900
Open access books available

186,000
International authors and editors

200M
Downloads

Our authors are among the

154
Countries delivered to

TOP 1%
most cited scientists

12.2%
Contributors from top 500 universities

WEB OF SCIENCE™

Selection of our books indexed in the Book Citation Index in Web of Science™ Core Collection (BKCI)

Interested in publishing with us?
Contact book.department@intechopen.com

Numbers displayed above are based on latest data collected.
For more information visit www.intechopen.com

Chapter

Synthesis and Characterizations of Titanium Tungstosilicate and Tungstophosphate Mesoporous Materials

Mohamed A. Ghanem, Abdullah M. Al-Mayouf and Mabrook S. Amer

Abstract

The work reports a development approach for the synthesis of novel multi-components mesoporous materials of titanium tungstate (*meso*-TiW) titanium tungstosilicate (*meso*-TiWSi) and tungstophosphate (*meso*-TiWP) mixed oxides that have high surface area and ordered mesoporous structures at nanometer length scale. Using the solvent evaporation-induced self-assembly (EISA) new oxides of bi- and tri-component of *meso*-TiW, *meso*-TiWSi and *meso*-TiWP oxides with different compositions and porosity were achieved. The physicochemical properties of the mesoporous oxides were characterized by X-ray diffraction, BET surface area analyzer, scanning, and transmission electron microscopes. Subject to the oxide composition, the obtained *meso*-TiW, *meso*-TiWSi and *meso*-TiWP exhibits high surface area, ordered 2D hexagonal mesostructured with order channels extended over a large area. The produced *meso*-TiW, *meso*-TiWSi, and *meso*-TiWP adsorbents exhibit good adsorption efficiency for the removal of Pb(II), Cd(II) and Hg(II) ions from water solution due to the presence of high surface area and accessibility of surface active sites. The adsorption efficiency of these mesoporous oxide reaches up to 95% and is found to be dependent contact time and adsorbents dose. The synthesis strategy is particularly advantageous for the production of new complex (multi-component) inorganic mesoporous materials that might have an application in the field of environmental, catalysis or energy storage and production.

Keywords: mesoporous, titanium tungstosilicate, tungstophosphate, surfactant self-assembly

1. Introduction

The approaches used for the synthesis of nanostructured materials show a critical role in synthesis the required materials and determining its final properties. To achieve mesoporous inorganic oxide powders with high surface area, uniformity and even mesoporous structures, there are many protocols have been implemented [1, 2] and the most important ones are: mesoporous silica materials as a host [3, 4],

sol-gel precipitation, solution co-precipitation, thermal solid state, and surfactant self-assembled templates [5–8]. Generally, the sol-gel precipitation, co-precipitation, and surfactant self-assembled templates were the most widely used methods for preparation of mesoporous ion exchange materials.

The synthesis of nonsiliceous nanostructured mesoporous materials with high surface area using surfactant self-assembled templates has been recognized as a method for controlling the phase structure, ordering and pore size of these functional materials [9–12]. A wide range of mesoporous oxides, metals and semiconductors materials with regular geometries have been successfully prepared by direct templating from liquid crystalline phases [13]. Nevertheless the synthesis of nonsiliceous mesostructured still lags behind the synthesis of mesoporous silica materials, particularly for complex and multi-components inorganic materials. The reasons for this come from the complexity, reactivity, chemical stability and interaction of the surfactant with the inorganic precursor. Establishment of synthetic routes for multi-component metal oxide mesostructured those are effective, applicable, reproducible and suitable for large-scale production still remains a challenge.

Inorganic ion exchange materials are widely used for water treatment, in the semiconductor industry, and in nuclear technology. Multi-component ion-exchange materials, such as titanium tungstosilicate (TiWSi) and tungstophosphate (TiWP) mixed oxides have better chemical and thermal stability and exchange capacity compared to Ti (IV) tungstate, Ti (IV) silicate and Ti (IV) phosphate. The crystalline phases of these materials have been utilized for separating heavy metals in aqueous media. The adsorption, separation and exchange properties of these systems could potentially be enhanced significantly if the materials were obtained with mesoporous structures.

In this work, the solvent evaporation-induced self-assembly (EISA) template method is adapted to produce a selection of mesoporous ion exchange materials such as titanium tungstate (*meso*-TiW) titanium tungstosilicate (*meso*-TiWSi) and tungstophosphate (*meso*-TiWP) mixed oxides with the high surface area and controlled porous structures that similar to mesoporous silica. Using this method mesoporous ionic exchange materials can be synthesized with homogeneous and uniform structures in the form of powders, amenable to mass production, or as membranes depending on the conditions employed during the synthesis. The characterization and adsorption capacity of the resulting nanostructured mesoporous materials is investigated for water demineralization and the removal of heavy metal ions from water solution.

Using the template strategy to synthesize nanostructured mesoporous materials with a different shape, size and morphology was firstly introduced by Mobil scientists [14] and Martin *et al.* [15, 16]. In this template method, the desired materials are chemically formed using self-assembled surfactant templates (sol-gel) or electrochemically deposited inside the pores of a nanoporous membrane that subsequently dissolves away leaving a replica of nanomaterials structures. The templates are divided into two different types: hard and soft templates. The commonly used hard templates include anodic aluminum oxide [16], silica [17], and polystyrene spheres [18] and mesoporous carbon [19]. The soft templates are formed from surfactant molecules that are self-assembled into organized mesophases (soft matter) that are intermediate in order between crystalline solids and isotropic liquids.

In recent years, the sol-gel process is widely utilized concurrency with organic-directed assembly to synthesize a variety of non-siliceous mesostructured materials such as transition metals, metal oxides, semiconductors, carbons, and polymers. Such mesostructured materials have attracted significant attention because of the application of these materials in nanoscale devices, sensors, microelectronic devices, catalysts, energy storage media, and adsorbent materials. Mesoporous silica-based materials, for example, have been widely attracted an attention for heavy metal ions adsorption from wastewater [20–23]. This because they exceptionally have the large

specific surface area, regular pore structure, and tunable pore sizes. Consequently, the mesoporous materials are expected to exhibit better heavy metal ions adsorption due to improved accessibility to the adsorption sites and/or speeding up the diffusion process within the mesopores. Toward this end and very recently, mesoporous silica materials were prepared by microwave assistant heating using silica fume as silica source and evaluated as adsorbents for the removal of Cu^{2+}, Pb^{2+}, and Cd^{2+} from aqueous solutions [24]. The results showed that the produced mesoporous silica could efficiently confiscate the heavy metal ions from aqueous solution within pH range of 5–7 and the maximum removal capacities of the mesoporous silica for Cu^{2+}, Pb^{2+}, and Cd^{2+} were 36.3, 58.5, and 32.3 mg/g, respectively.

In addition, mesoporous silica modified with suitable organic functional groups have shown enhanced heavy metals adsorbents capacity due to combining the open porous structure of mesoporous silica with suitable organic compounds that exhibit high binding affinity toward the target metal ions. As an example, Lee *et al.* [22] reported the adsorption of Pb(II) and Cu(II) metal ions on mesoporous silica modified with organic amine and thiol functional groups and results reveal that the thiol-functionalized mesoporous silica adsorbents exhibit enhanced adsorption affinity for Pb^{2+} than the amino-mesoporous silica. Moreover, other studies reported an excellent Hg removal efficiency on thiolated mesoporous silica compared to the aminated ones [23, 25].

Sol-gel process using polyethylene oxide (PEO) as well as low molecular weight surfactants have been adapted for the preparation of thermally stable, ordered and large pore size mesoporous non-silica materials of metal oxides including MnO_2, TiO_2, ZrO_2, Nb_2O_5, Ta_2O_5, Al_2O_3, SnO_2, WO_3, HfO_2, and mixed oxides of Al_2TiO_y, $ZrTiO_y$, ZrW_2O_y [26–28]. The pore topology and pore size of the mesoporous oxides can be controlled by varying the surfactant or by the addition of hydrophobic swelling agents to the template mixture. However, the nature of the inorganic precursors of transition metals plays a critical for this process and it has to be compatible with organic co-assembly [29]. Therefore the evaporation-induced self-assembly (EISA) was introduced for the synthesis of non-silica mesostructured materials and has shown to be the very useful approach for both controlling macroscopic form (powder, thin films, and membranes) and mesostructured [30, 31]. In this EISA process, the mixture of volatile solvent, (commonly ethanol) surfactant and inorganic precursors are exposed to evaporation which drives the co-assembly of surfactant molecules and inorganic precursors to form the ordered mesophases. Subsequently using aging, chemical or heat treatments induce the formation of the desired mesostructures. Recently mesostructures of titanium tungstate with the high surface area, large pore volume, uniform pore size, and tunable W/Ti ratios were successfully fabricated by using (EISA) strategy [32]. Also, mesoporous zirconium phosphotungstate with large specific surface area ~170 m^2/g, large pore volume, uniform pore size distribution, and tunable W/Zr ratios were prepared by adopting this EISA method [33]. In another template strategy, mesoporous TiO_2/WO_3 hollow fibers and interconnected nanotubes are prepared by hollow fibers as a framework, in addition, to block copolymer as a template. The mesostructures showed a surface area of ~130 m^2/g with improved photodegradation activity [34].

Earlier studies on the synthesis of inorganic ion-exchangers are well documented by Amphlet [35] and Clearfield [36]. A comprehensive review of inorganic ion-exchangers with layered structures [37] has been published which suggests that group IV phosphates, molybdates, tungstates, etc. possess interesting cation-exchange properties. Silicates of Ti(IV) have been shown to have porous properties and are being used as molecular sieves [38]. Two new crystalline phases of α-titanium phosphates with layered structures have been reported [39]. Siddiqui *et al.* [40] have synthesized crystalline phases of titanium tungstosilicate (TiWSi)

and titanium tungstophosphate (TiWP) with better ion exchange capacity and better chemical and thermal properties as compared to titanium phosphate, titanium tungstate, and titanium silicate. Furthermore, ion-exchange materials with the amorphous state, crystalline state, and hybrid organic-inorganic states have been recently synthesized and studied for environmental applications [41, 42].

2. Experimental

2.1 Chemicals and materials

Triblock poly(ethylene oxide)-b-poly(propylene oxide)-b-poly-(ethylene oxide) copolymer Pluronic® P123 ($EO_{20}PO_{70}EO_{20}$, Mw = 5800, Sigma-Aldrich) was used as the structure-directing agent (SDA) and titanium tetraisobutoxide ($Ti(OBu)_4$, 98%, Aldrich), tungsten hexachloride WCl_6, phosphorus pentachloride PCl_5 (reagent grade, 95%, Sigma-Aldrich) and tetraethyl orthosilicate (TEOS, 98%, AnalaR) were used as Ti, W, P and Si source respectively. *n*-Propanol ($n\text{-}C_2H_8O$, BDH AnalaR) was used for dissolve the surfactant and hydrochloric acid HCl (37 wt. %, Analar) were all supplied by Shanghai Chemical Corp. Copper(II) nitrate hydrate, lead(II) nitrate (ACS reagent, ≥99.0%) and mercury(II) nitrate monohydrate (ACS reagent, ≥98.0%) are purchased from Sigma-Aldrich. All other chemicals were used as received without further purification and all aqueous solutions were prepared using Milli-Q (Millipore, Inc.) high quality deionized (DI) water (resistance 18.2 MΩ cm).

2.2 One-pot synthesis of bi-components mesoporous titanium tungstate (meso-TiW-x) using EISA approach

Mesoporous bi-components titanium tungstate (*meso*-TiW-x) oxides were synthesized with different composition through a modified evaporation-induced self-assembly (EISA) method. Typically, with a total Ti-W molar content of 18 mmol, $Ti(OBu)_4$ and WCl_6 were first dissolved in a mixture containing 20 g of *n*-propanol and 2.0 g of Pluronic 123 ($EO_{20}PO_{70}EO_{20}$). Then, the mixture was allowed for stirring for 2.0 hours at room temperature in a sealed vial. The obtained sol was cast into Petri dishes and kept under ambient conditions for 1 hour as shown in **Scheme 1**. Subsequently, the as-made gel was cured at 40°C for 2 days and then calcined in flowing air at 400°C for 4 hours with a ramping rate of 1°C min^{-1}. The obtained samples of *meso*-TiW were denoted as *meso*-TiW-x, where X equals 20, 30, and 40 wt. % the percentage of W in the original template mixture.

Specifically, for the synthesis of *meso*-TiW-20, *meso*-TiW-30 and *meso*-TiW-40, a 4.90, 1.43, 4.28 g of $Ti(OBu)_4$ were added to 2.14, 3.68, 2.86 g of WCl_6, respectively. In order to further moderate the hydrolysis rate, a 1.20 g of hydrochloric acid (37 wt. %) was added to the solution for synthesizing *meso*-TiW-20 oxides. A control experiment was performed to prepared pure *meso*-TiO_2 using EISA approach for comparison purpose.

2.3 Synthesis of mesoporous titanium tungstosilicate (meso-TiWSi) and titanium tungstophosphate mixed oxides (meso-TiWP)

The mesoporous titanium tungstosilicate oxides (*meso*-TiWSi-x, where x is equal 5, 10, 15, 20, 40, 60 wt. % the percentage of Si in the original template mixture) and titanium tungstophosphate mixed oxides *(meso*-TiWP-x, where x is the wt. % of P in template mixture equal 5, 10, 15, 20 and 30 wt. %) were synthesized through

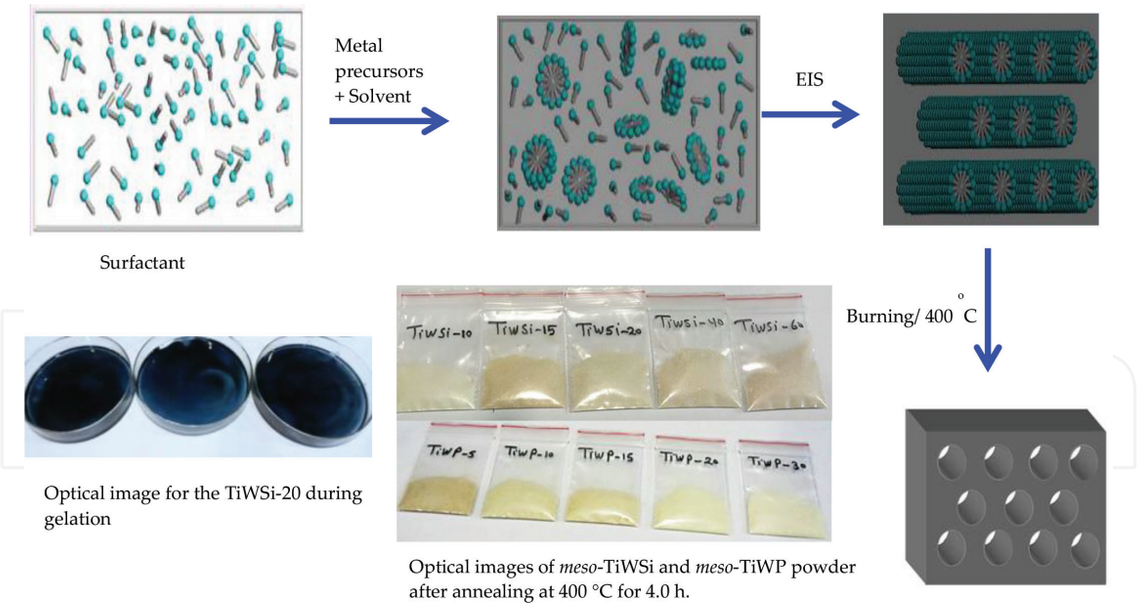

Scheme 1.
Schematic diagram for the synthesis of mesoporous materials of titanium tungstate (meso-TiW) titanium tungestophosphate (meso-TiWP) and titanium tungstosilicate (meso-TiWSi) by EISA.

adopted (EISA) method as shown above in **Scheme 1**. In a typical experiment, 2.86 g of WCl_6 was dissolved in 10 g of *n*-propanol, this mixture was mixed by stirring until getting the clear solution then 3.68 g of $Ti(OBu)_4$ was added to this solution to obtain a solution (A). Then 2.0 g of nonionic surfactant (triblock copolymer templates (P®123), was dissolved in 10 g *n*-propanol and stirred for 10 min and different amounts of TEOS (5, 10, 15, 20, 40, 60 wt. %) were added to this solution and stirring for another 5.0 min to obtain a solution (B). In case of titanium tungstophosphate 5, 10, 15, 20 and 30 wt. % of PCl_5 was added to this solution and stirring for 5 min to obtain solution B. The solution (A) was added dropwise to (B) then the mixture was stirred for 2.0 hours at room temperature in a sealed vial. In order to further moderate the hydrolysis rate, 1.20 g of hydrochloric acid (37 wt%) was added to the solution for all prepared mixtures of mesoporous *meso*-TiWSi oxides. The obtained dark-blue colored homogeneous solution (shown in the inset in **Scheme 1**) was cast into Petri dishes and kept under ambient condition for 1.0 hour. Subsequently, the as-made gel was cured at 40°C for 2 days to completely remove solvents. Finally, the blue deposit was scraped and crushed into powder and then calcined in flowing air at 400°C for 4.0 hours with a ramping rate of 1.0°C/min.

2.4 Materials characterizations

X-ray powder diffraction (XRD) and Small-angle X-ray (SAXS) measurements were recorded respectively on a Bruker D4 powder X-ray diffractometer (Germany) and Nanostar U small-angle scattering system (Bruker, Germany) by using Cu K_α radiation (40 kV, 40 mA). The BET surface area, pore volume, and the pore size distributions were measured by nitrogen adsorption/desorption using a Micromeritics Tristar 3020 analyzer (USA). Prior to the measurements, the samples were degassed at 180°C for at least 6.0 hours. The Brunauer-Emmett-Teller (BET) method was utilized to calculate the specific surface area. By using the Barrett-Joyner-Halenda (BJH) model, the pore volumes and pore size distributions were derived from the adsorption branches of isotherms. Transmission electron microscopy (TEM) analysis was conducted on a JEOL 2011 microscope (Japan) operated at 200 kV and equipped with an energy dispersive X-ray (EDX) detector. Field-emission

scanning electron microscopy (FESEM) images were collected on the Hitachi Model S-4800 field-emission scanning electron microscope. The heavy metals analysis was performed using an inductively coupled plasma optical emission spectroscopy (ICP-OES) system (Thermo Scientific; UK, Model ICAP 6000).

2.5 Procedure for heavy metal ions adsorption from water by mesoporous materials

The standard procedure for the removal of heavy metal ions from water using the produced mesoporous materials was performed by mixing a weighted amount of the mesoporous absorbent with 3.0 mL solutions containing 0.2 mg/L Cu(II), Cd(II) or Pb(II) nitrate salt in polypropylene tubes. The samples were placed in a shaking water bath at 25°C for 2.0 hours and then the solution was separated by centrifuge at rpm 7000 for 10 min in each run. Each solution was then diluted by taking 100 μl and transferred into 10 mL conical polypropylene flask for analysis by ICP. The amount of metal ion adsorbed at the mesoporous adsorbents was calculated by the difference of the initial concentration (C_o) and the equilibrium concentration (C_e). The removal efficiency and equilibrium adsorption capacity of Cd(II), Pb(II), and Hg(II) ions from the solution was calculated using the following equations:

$$(E\%) = (C_o - C_e/C_o) \times 100 \quad (1)$$

$$(Q_e\%) = (C_o - C_e)\, V/m \quad (2)$$

Where, E, Q_e, C_o, C_e, V, and *m* are the removal efficiency, equilibrium adsorption capacity (mg/g), initial concentration (mg/L), equilibrium concentration (mg/L), solution volume (L) and adsorbent mass (g) respectively. To investigate metal ion loss during the adsorption due to the glassware or any of the experimental equipment a parallel experiment was performed in the absence of the mesoporous adsorbents and it was regarded as a standard solution.

3. Results and discussion

3.1 Synthesis and characterizations of bi-components meso-TiW prepared by EISA approach

In this section, we present the result for the synthesis of bi-components *meso*-TiW with various ratios using modified solvent evaporation-induced self-assembly (EISA). Firstly the synthesis of bi-components of mesoporous titanium tungstate (*meso*-TiW) with various compositions was executed. In EISA process the mixture of volatile solvent, (commonly ethanol), copolymer surfactant and inorganic precursors are mixed together and exposed to evaporation which drives the co-assembly of surfactant molecules and inorganic precursors to form the ordered mesostructures. The W content was varied between 20 and 40 moles and the *meso*-TiW powder after annealed at 400°C for 4.0 hours shows the light yellow color crystal as such shown in the inset of **Scheme 1** which indicating on the precipitation of TiW oxide while pure *meso*-TiO_2 exhibits white color.

Figure 1 shows the wide-angle XRD patterns for *meso*-TiW-20 and for pure *meso*-TiO_2 prepared using EISA approach for comparison purpose. The XRD pattern of pure *meso*-TiO_2 displayed a well-crystallized anatase phase (JCPDS Card No. 01-083-2243), while for *meso*-TiW-20 the XRD peaks intensity is slightly decreased

in addition to the disappearance of some other peaks. This can attribute to the addition of 20 wt. % of W precursor hinders the crystallization of anatase phase and instead an amorphous composite of Ti—W oxides were formed.

The nitrogen adsorption-desorption isotherms and the plot for pore size distribution of the mesoporous TiW-x oxides are shown in **Figure 2**. From the isotherms we can see that the *meso*-TiW oxide showed typical type IV isotherms with sharp capillary condensation steps at a relative pressure (P/P^o) of 0.35–0.85 that characteristic for mesoporous materials.

The average pore size, surface area (BET), pore volume for the *meso*-TiW oxide sample in comparing with pure mesoporous TiO_2 (prepared using EISA approach but without adding WCl_6) are shown in **Table 1**. Obviously, the *meso*-TiW-30 oxide shows the highest surface area; lower pore volume and a narrow pore size distribution which demonstrates the formation of highly ordered and uniform mesoporous structure. On the other hand, the pure mesoporous TiO_2 prepared in absence of WCl_6 shows lower surface area (81 m^2/g) and higher pore volume with bimodal pore diameters. This can be attributed to the incorporation of W precursor effectively improve the order of mesoporous structure and because of the tungsten oxide has a high density (7.16 g/cm^3) the incorporation of W leads to slightly reduce the pore volume of *meso*-TiW oxide.

Figure 3 shows the TEM image of the mesoporous *meso*-TiW samples. Clearly, the fine structure of the *meso*-TiW oxides shows typical morphologies of the highly ordered 2D hexagonal mesostructures with highly orderly channels extended over large domains which are consistent with high surface area obtained by N_2 adsorption results and confirms the successful production of bi-components mesoporous TiW oxides by EISA approach.

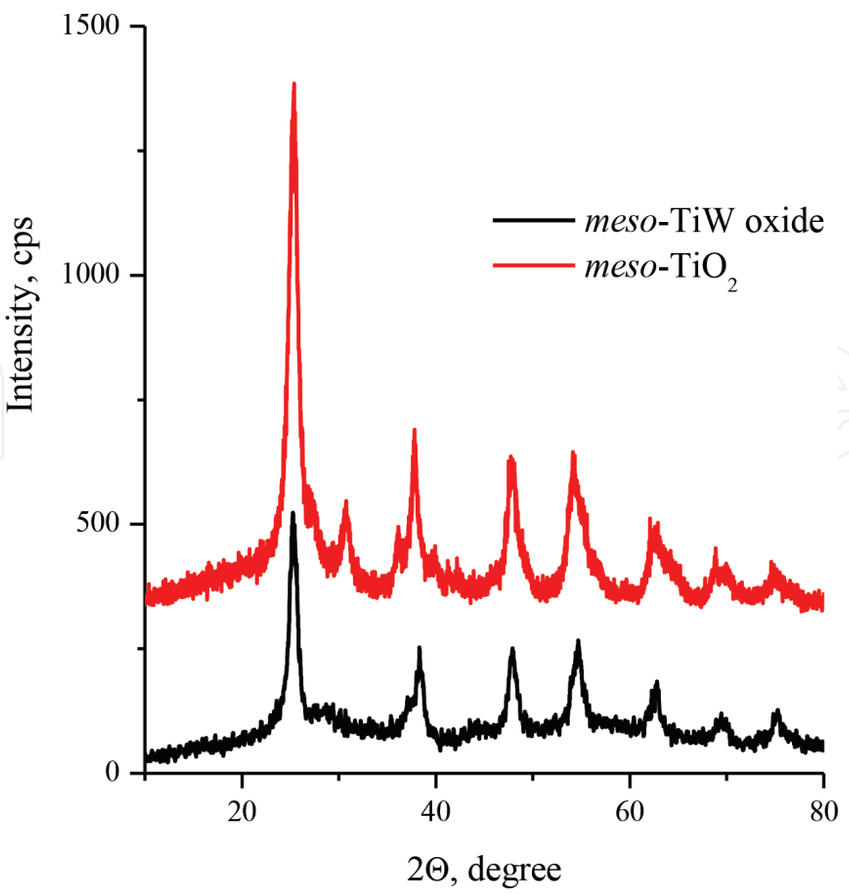

Figure 1.
X-ray diffraction patterns for meso-TiW-20 and pure meso-TiO_2 prepared by EISA approach and annealed at 400°C, 4.0 hours.

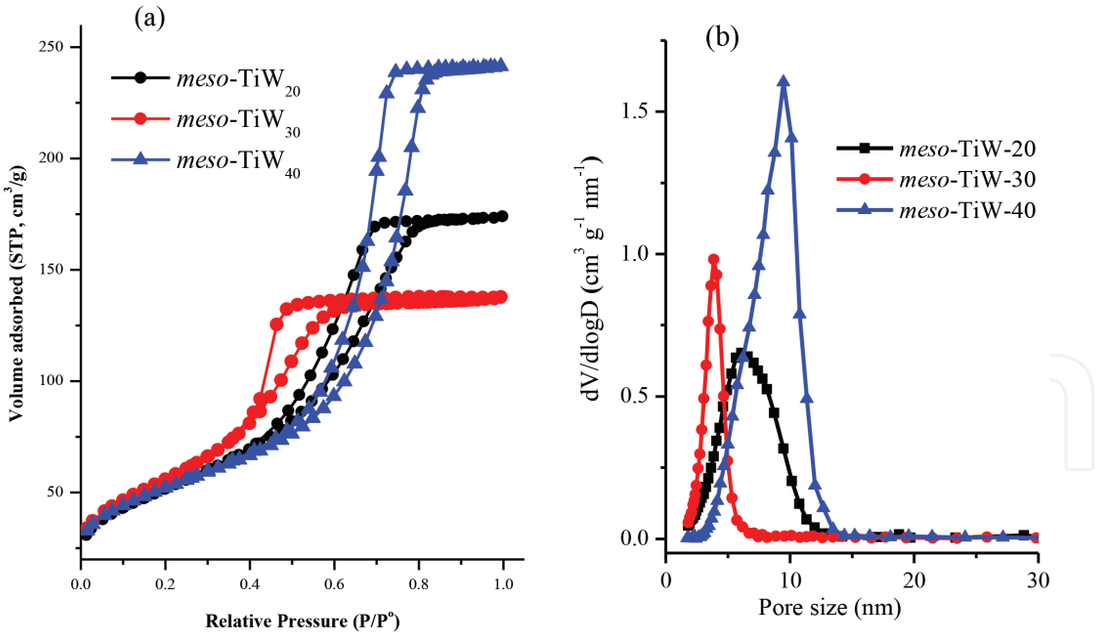

Figure 2.
(a) Nitrogen adsorption-desorption isotherms, (b) the corresponding pore size distribution curves of the meso-TiW oxide.

Samples	SBET (m^2/g)	Pore volume (cm^3/g)	Pore size (nm)
meso-TiW-20	189	0.27	6.1
meso-TiW-30	206	0.21	3.9
meso-TiW-40	188	0.37	9.5
meso-TiO_2	81	0.33	6/12.5

Table 1.
The textural properties of the samples of mesoporous TiW oxides.

3.2 Synthesis and characterization of tri-component mesoporous titanium tungstosilicate (meso-TiWSi) materials

Here we investigate the possibility of synthesis more complicated mesoporous materials of tri-components mesoporous oxides of Ti, W, and Si. Because the bi-components *meso*-TiW-30 showed the highest surface area (206 m^2/g) and ordered pore structure we used its composition of mole ratio ($Ti_{70}W_{30}$) as start material for the synthesis of tri-component mesoporous titanium tungstosilicate *meso*-TiWSi-x and tungstophosphate (*meso*-TiWP-x) materials with various compositions of silica (x = 10, 15, 20, 40 and 60 wt. %) via the facile EISA method employing P®123 surfactant, $Ti(OBu)_4$, WCl_6 and TEOS as described in Section 2 above and shown in **Scheme 1**. Optical images of the produced *meso*-TiWSi materials with Si ratio of 10, 15, 20, 40 and 60 wt. % after annealing at 400°C in the air are shown in the inset of **Scheme 1**.

Figure 4 shows the low-angle and wide-angle X-ray diffraction patterns of mesoporous *meso*-TiWSi-x calcined at 400°C in the air. As shown in **Figure 4a**, there's a distinct peak at 2θ = 0.53°can be observed which is indexed as (100) reflections characterize of the 2D hexagonal mesostructure [32, 43]. Furthermore, another one broad and weak diffraction peak can clearly observe at 2θ = 1–1.5° indicates the long-range order of the mesopores structure. An increase in the Si ratio up to 60 wt. % result in one broad peak can be seen in the SXRD diffraction pattern, suggested that an excessive increase in Si incorporation decreased the ordering of the mesoporous structure. For the TiWSi-10, the first scattering peak shifts from a 0.53 nm^{-1} to

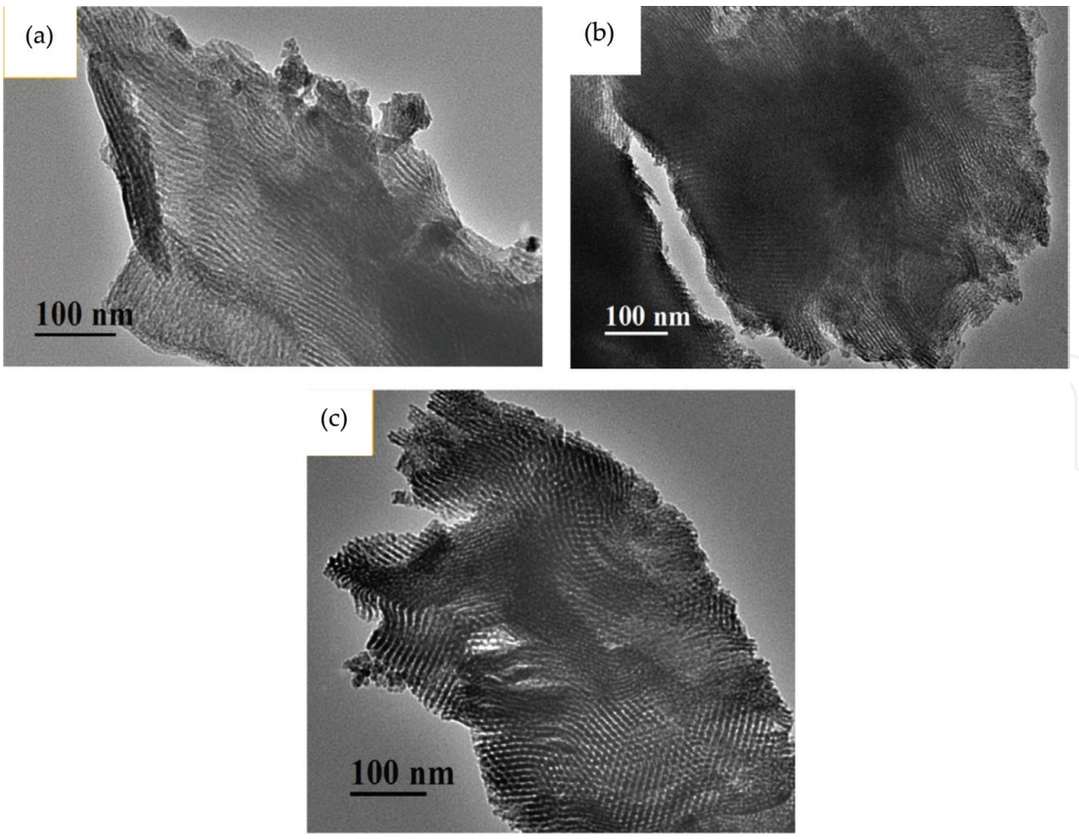

Figure 3.
TEM images of the samples (a) meso-TW-20, (b) meso-TW-30, and (c) meso-TW-40.

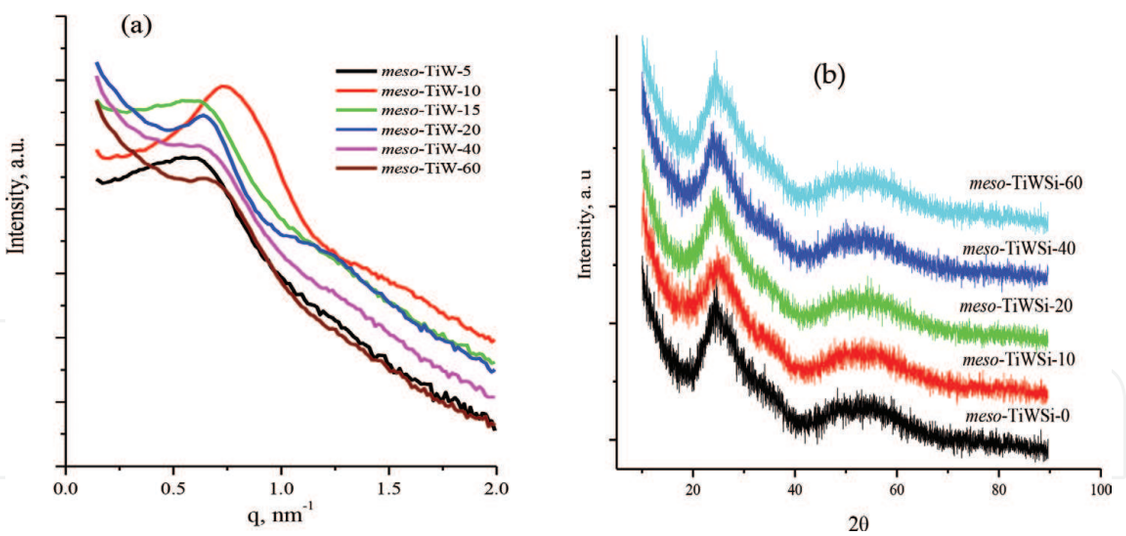

Figure 4.
(a) Low-angle and (b) wide-angle X-ray diffraction patterns of mesoporous meso-TiWSi-x calcined at 400°C in the air for 4.0 hours.

a larger q value of a 0.56 nm^{-1}, corresponding to the framework shrinkage during the removal of the template. The wide angle X-ray diffraction (WXRD) patterns of these samples are shown in **Figure 4b**. All the patterns kept consistent with each other and only exhibited two broad peaks in the 2θ range of 20–40° and 40–60°, indicating the existence of an amorphous or semicrystalline mesoporous TiWSi wall structure. No individual crystalline peak of titanium tungstate or titanium was observed.

Meanwhile, there were no peaks of tungsten oxide in the patterns, illustrating the high dispersion of tungsten and silicon oxide among the mesoporous framework even in *meso*-TiWSi-0, which had silica ratio of 0 wt. %. This might be accounted

to the silica atoms in the materials were segregated by titanium and tungsten atoms due to the advantage of using the one-pot EISA method [44]. We presumed that the presence of W and Si species somehow retarded the crystallization of TiO_2 during the calcination and hence benefited the preservation of the ordered mesostructured which is consistent with **Figure 4b** and the previous studies [45, 46].

In order to further confirm the presence of mesopores in *meso*-TiWSi-x materials, the SEM and TEM characterizations were performed and **Figure 5** shows the SEM images of the *meso*-TiWSi-x samples with different Si ratios after the annealing process. For the *meso*-TiWSi-10 (**Figure 5a**) and *meso*-TiWSi-20 (**Figure 5b**), the SEM images clearly show the highly ordered mesopores uniformly exist through the TiWSi framework over a wide micrometer area. However for *meso*-TiWSi-40 and *meso*-TiWSi-60, the SEM images in **Figure 5c** and **d** show wormlike mesoporous structure indicating on less order pore arrangement when Si ratio is increased to 60 wt. %.

Figure 6 shows the TEM images for different composition of *meso*-TiWSi after calcination and obviously, the TiWSi framework exhibits a 2D hexagonal mesostructured with ordered mesopores of about 10 nm in diameter. It also clearly observes the existence of ordered pores along the [110] and [001] directions in **Figure 6b** of *meso*-TiWSi-20. Nevertheless by further increasing the Si ratios to 60 wt. % (**Figure 6d**), the structure showed wormlike mesoporous channels rather than the long-range ordered hexagonal pores. The results of SEM and TEM agreed quite well with the results of the SXRD characterization, which predicted the presence of ordered mesoporous structure for samples with Si ratio from 0 to 20% and wormlike mesopores structure for meso-TiWSi-60.

For the elemental composition analysis, the backscattering SEM image and energy-dispersive X-ray (EDX) analysis of the elemental composition of the *meso*-TiWSi-20 materials are shown in **Figure 7**. The backscattering SEM image (**Figure 7a**) obviously shows very and highly order channels running through the *meso*-TiWSi framework confirming the formation of long-range and ordered

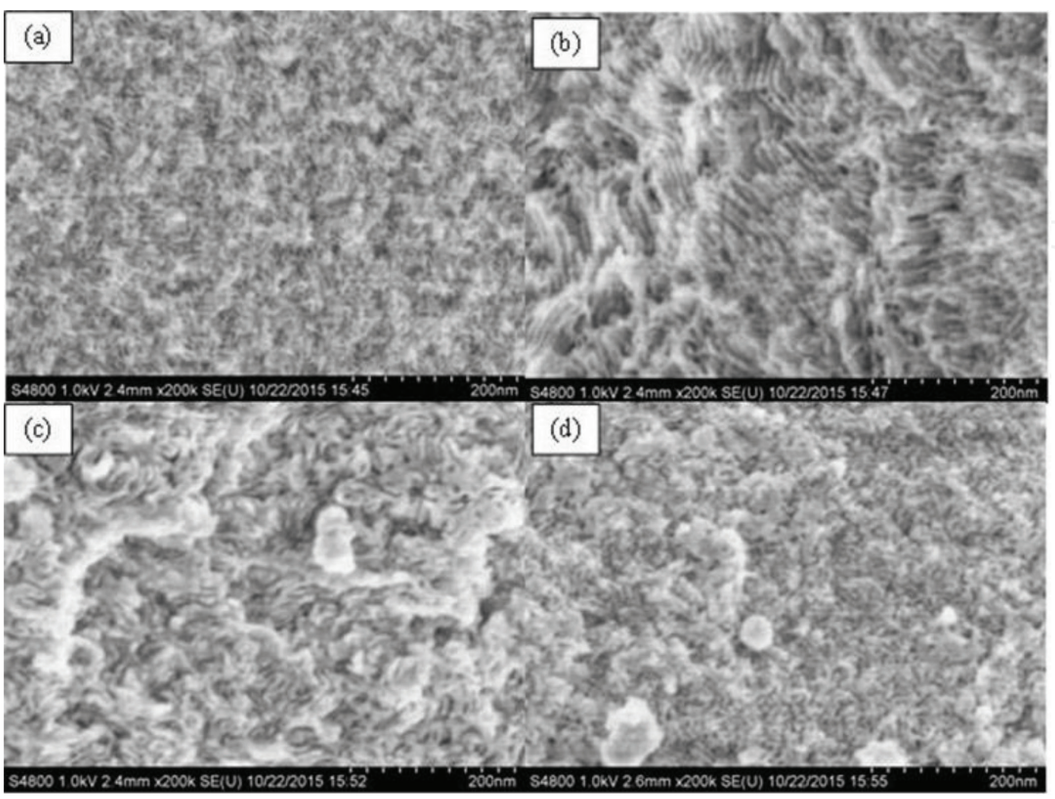

Figure 5.
SEM images of (a) meso-TiWSi-10 (b) meso-TiWSi-20 (c) meso-TiWSi-40 (d) meso-TiWSi-60.

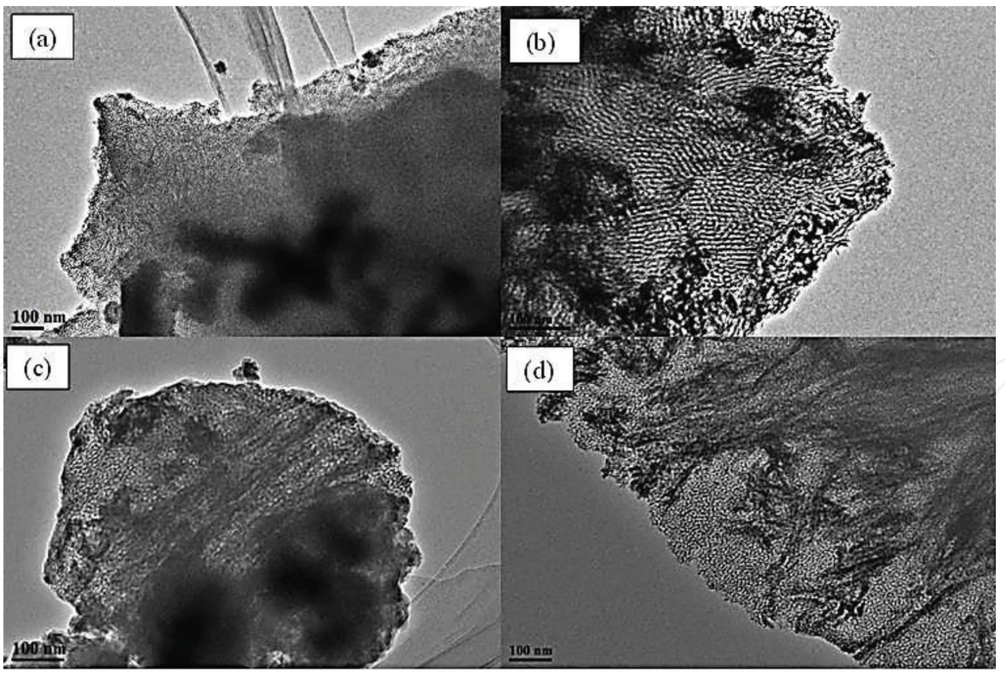

Figure 6.
TEM images of (a) meso-TiWSi-10 (b) meso-TiWSi-20 (c) meso-TiWSi-40 (d) meso-TiWSi-60.

mesopores. The EDX elemental analysis in **Figure 7b** shows evidently the existence of Ti, W, O and Si elements approving that all the elements were successfully introduced into the framework of the mesoporous structure. The Si wt. % derived from the EDX analysis were very close to the target composition set up in the template mixture as shown in **Table 2**.

The textural properties and the surface area of the ordered *meso*-TiWSi-x with different Si ratios were characterized by the N_2-physisorption technique. Nitrogen adsorption and desorption isotherms and the corresponding pore size distributions of the *meso*-TiWSi materials are shown in **Figure 8**. For all the materials, the isotherms exhibited typical type IV isotherms and well-defined H_2 shaped hysteresis loops with sharp capillary condensation steps at a relative pressure (P/P^o) of 0.4–0.8, that characteristic of mesoporous materials [45, 47]. Besides, all the capillary condensation steps of the hysteresis loops for all the samples were very steep, pointing to the presence of a uniform and ordered pore size in the framework of *meso*-TiWSi. The average pore size of these samples was narrowly distributed at around 4–10 nm, implying the existence of the uniform mesoporous channels within the obtained materials. The details textual parameters including specific surface area, pore size and volume of *meso*-TiWSi-x obtained from the N_2 adsorption-desorption isotherms, are summarized in **Table 3**. Clearly, all the samples

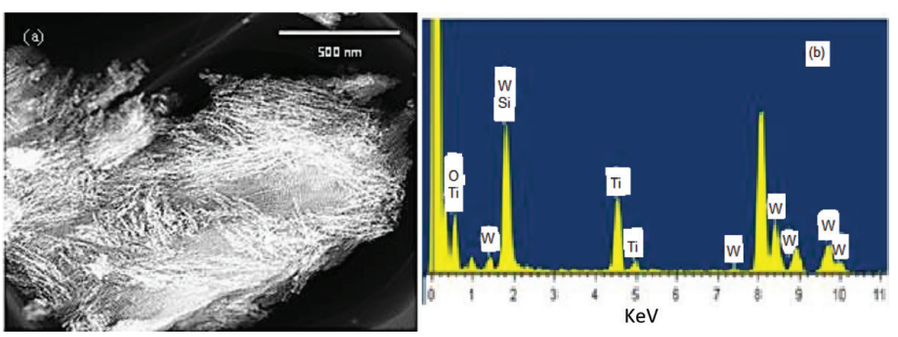

Figure 7.
(a) Backscatter SEM image of meso-TiWSi-20 (b) EDX elemental profile of meso-TiWSi-20.

Samples	Si wt. %
meso-TiWSi-10	7.4
meso-TiWSi-20	18.4
meso-TiWSi-60	54.3

Table 2.
EDX analysis of the Si wt. % in the meso-TiWSi samples.

had excellent textural properties with large specific surface area (131–188 $m^2\ g^{-1}$), uniform pore size (4–10 nm) and pore volume (0.17–0.37 $cm^3\ g^{-1}$).

3.3 Synthesis and characterization of tri-component mesoporous titanium tungstophosphates (meso-TiWP-x) materials

Tri-components mesoporous titanium tungstophosphates *meso*-TiWP-x materials were fabricated via the facile EISA method employing P®123 surfactants as a template and $Ti(OBu)_4$, WCl_6 and PCl_5 as precursor for Ti, W and P respectively. Starting with Ti: W mole ration of 70:30, various compositions of P (5, 10, 15, 20 and 30 wt. %) were incorporated into the *meso*-TiW-30 and an optical image of the produced *meso*-TiWP-x samples is shown in the inset of **Scheme 1**.

Figure 9 shows the small and wide angle X-ray diffraction pattern of *meso*-TiWP-x samples after annealing at 400°C for 4 hours. As indicates in **Figure 9a** there's a broad scattering peak in the 2θ range 0.5–1° which indicates on the formation of less ordered mesoporous TiWP structures. However, the *meso*-TiWP-10 shows rather well-defined peak among the other samples; presumably, due to better order pores have been formed. The wide-angle X-ray diffraction patterns of the TiWP samples shown in **Figure 9b** are consistent with each other and only exhibited two broad peaks in the 2θ range of 20–30° and 40–60° which is evidence for the existence of an amorphous or semi-crystalline framework of mesoporous TiWP. Based on the above results it can be concluded that the produce *meso*-TiWP-x samples have amorphous and less order porous structures than in the case of TiWSi.

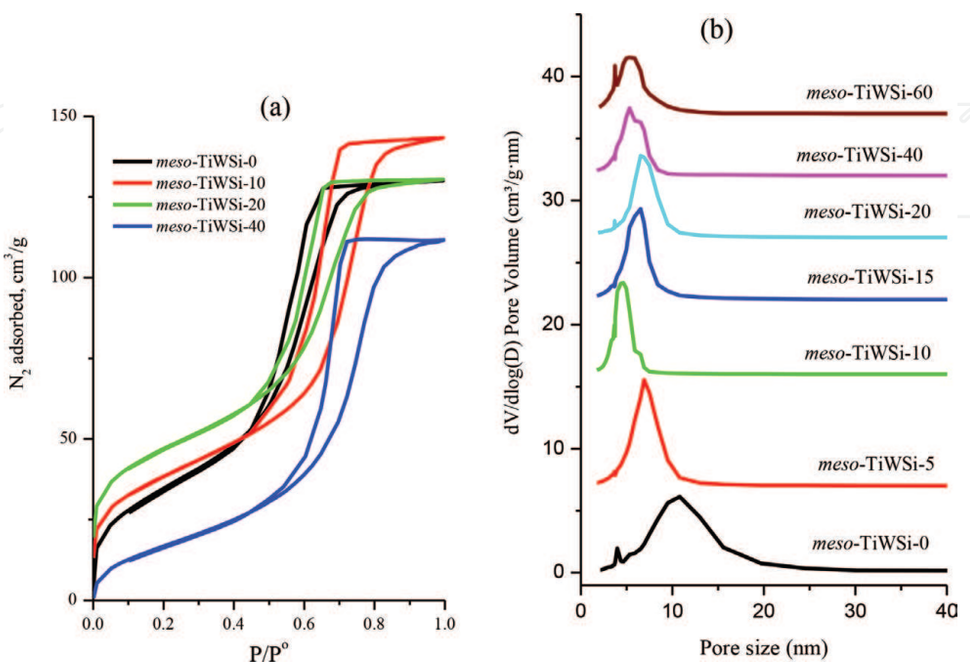

Figure 8.
(a) Nitrogen adsorption isotherms and (b) the corresponding pore size distribution curves of the meso-TWSi materials.

Samples	Specific surface area ± 5 ($m^2 g^{-1}$)	Pore size ±0.5 (nm)	Pore volume ($cm^3 g^{-1}$)
meso-TiWSi-0	188	9.5	0.37
meso-TiWSi-5	131	7.0	0.20
meso-TiWSi-10	164	5.5	0.19
meso-TiWSi-15	138	7.0	0.20
meso-TiWSi-20	142	7.5	0.22
meso-TiWSi-40	151	6.0	0.17
meso-TiWSi-60	156	5.0	0.19

Table 3.
Textural properties of the meso-TWSi-x materials derived from nitrogen adsorption and desorption analysis.

Figure 10 reveals the surface morphology of the *meso*-TiWP-x samples and by examining the SEM images, the formation of the pores are evidently observed within the TiWP framework and generally, the pores order seems to be irregular. However, for the *meso*-TiWP-10 sample, it shows some degree of ordered pores domains is formed. In addition the X-ray mapping and EDX composition analysis (not shown here) demonstrate the presence of Ti, W, P and oxygen elements which are uniformly distributed through the mesoporous TiWP materials.

The transmission electron microscope characterization of the *meso*-TiWP-x materials is illustrated in **Figure 11**. The TEM images of the mesoporous TiWP-x materials display large domains of the porous structure obtained after direct calcination at 400°C in the air due to the removal of templates. Clearly, the pores arrangement is rather random presumably due to the source of phosphor (PCl_5) affected the formation of the ordered mesostructured during the self-assembly process. However the TEM image for *meso*-TiWP-10 with phosphor content of 10 wt. % shows the pores are arranged in the highly ordered structure. It implies that adding phosphorus with 10 wt. % retains the pore order of the titanium tungstophosphates.

The N_2 adsorption/desorption isotherms of *meso*-TiWP-x materials after annealing at 400°C in the air are shown in **Figure 12a**. Evidently, the N_2 adsorption/

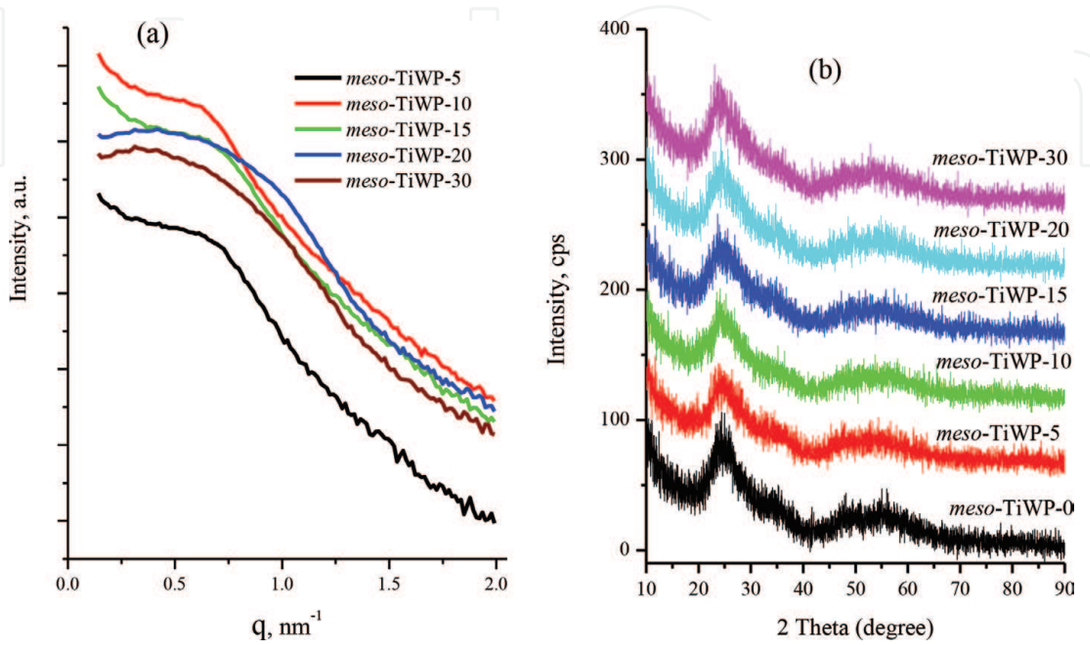

Figure 9.
X-ray diffraction patterns for meso-TiWP-x materials, (a) low angle and (b) high angle.

desorption isotherms for *meso*-TiWP-x materials show typical type IV curves with a sharp capillary condensation step at P/P^o = 0.8–0.9 and an H_2-type hysteresis loop, which is typical of large-pore mesoporous materials with cylindrical channels.

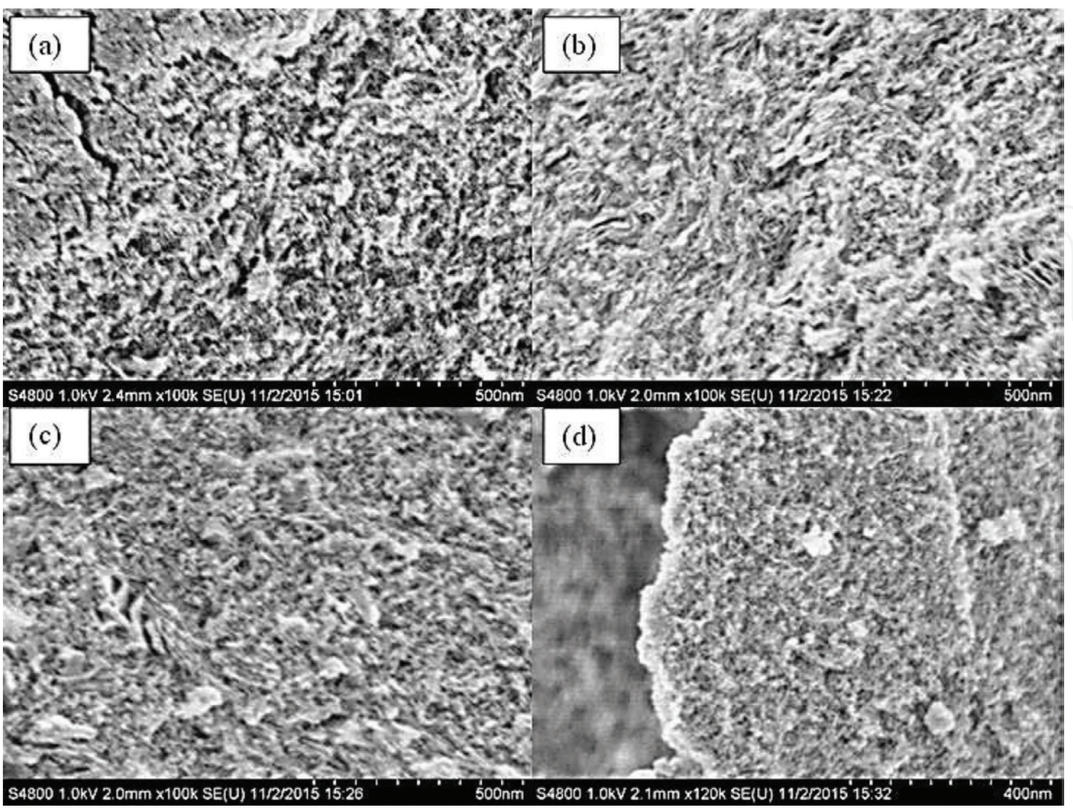

Figure 10.
SEM images of meso-TiWP-X: (a) meso-TiWP-5 (b) meso-TiWP-10 (c) meso-TiWP-15 (d) meso-TiWP-20.

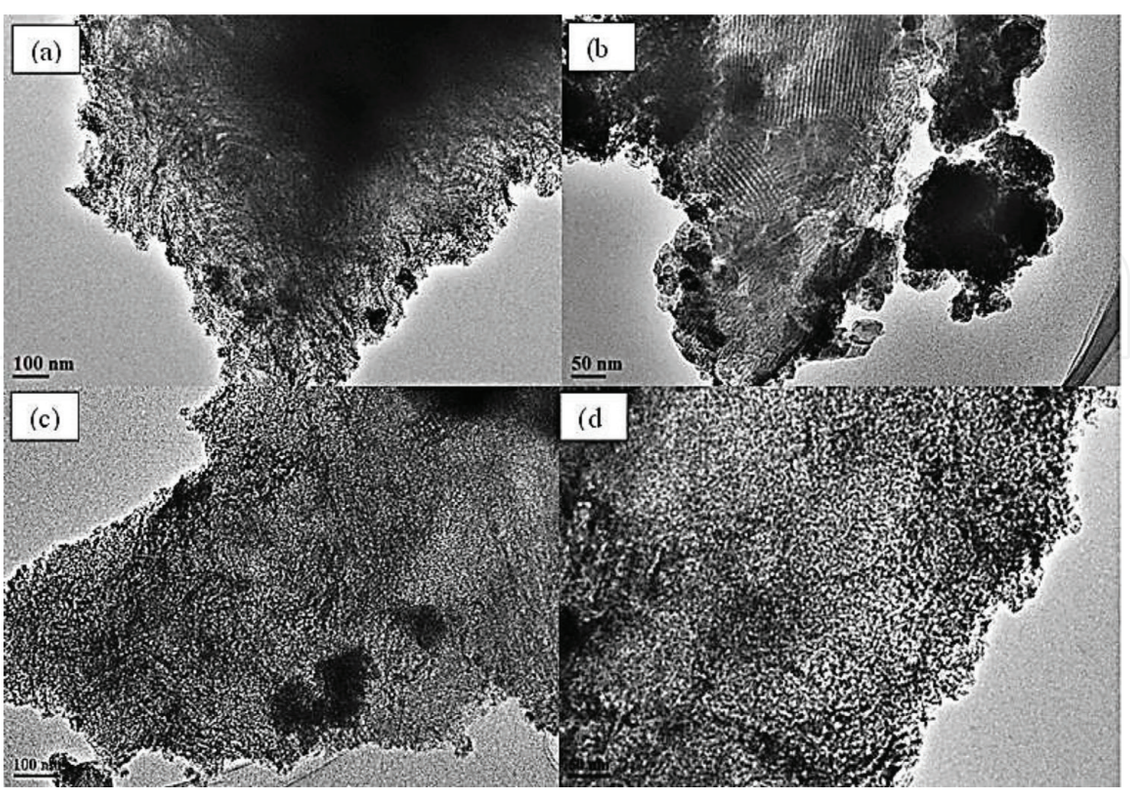

Figure 11.
TEM images of (a) meso-TiWP-5, (b) meso-TiWP-10, (c) meso-TiWP-15, (d) meso-TiWP-20 after annealing at 400°C in air for 4 hours.

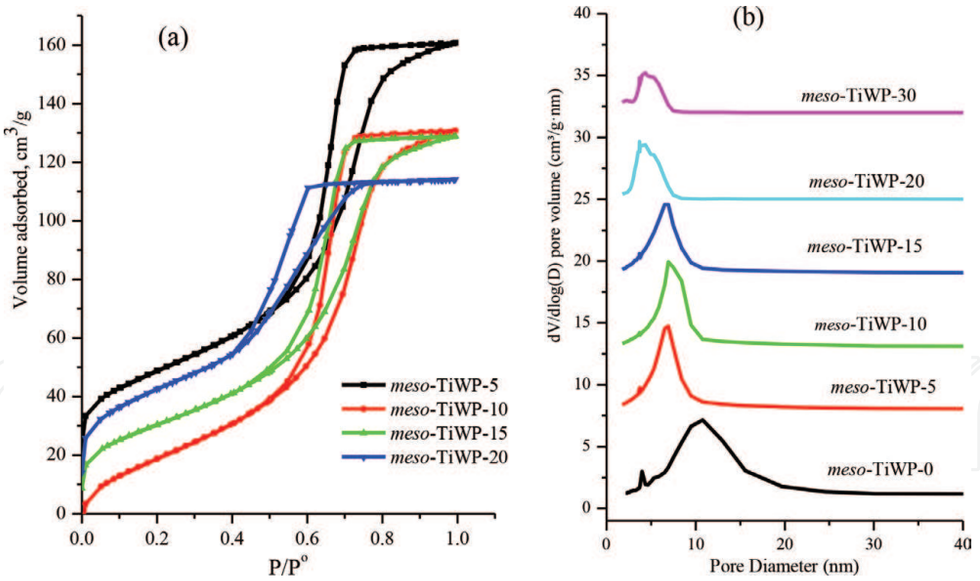

Figure 12.
(a) Nitrogen adsorption/desorption isotherms of meso-TiWP-x and (b) the corresponding pore size distribution curves.

The pore size derived from the adsorption branches of the isotherms by using the Barrett-Joyner-Halenda method is shown in **Figure 12b**. Generally, the pore diameter for the *meso*-TiWP-x materials shows a narrow distribution and a gradual decrease as the phosphorus content increases, with a pore diameter of 9.6 nm for *meso*-TiWP-0 and 4.3 nm for *meso*-TiWP-30 as reported in **Table 4**. The Brunauer-Emmett-Teller surface area and pore volume of the *meso*-TiWP-x materials are calculated from the N_2 adsorption/desorption isotherms and reported in **Table 4**. The BET surface area of the meso-TiWP-x materials is varied between 188 m^2/g for no phosphorus and a 128 m^2/g for *meso*-TiWP-15 which presumably due to the formation of the more crystalline mesoporous wall as the phosphorus is added to titanium tungstate. However, it can conclude that mesostructured of titanium tungstate can be retained during the addition of phosphorus and annealing treatment which confirms the versatility of EISA soft template approach to producing multi-components mesoporous oxides with various compositions.

3.4 Removal of heavy metal ions from water by mesoporous titanium tungstosilicate and tungstophosphate materials

This section reports the preliminary evaluation of the produced mesoporous materials for heavy metal ions removal from synthetic water solution. The ability

Material	Pore diameter/ nm	Pore volume/ $cm^3\ g^{-1}$	Specific surface area/ $m^2\ g^{-1}$
meso-TiWP-0	9.5	0.37	188
meso-TiWP-5	7.5	0.232	140
meso-TiWP-10	7.6	0.220	129
meso-TiWP-15	5.6	0.200	128
meso-TiWP-20	4.5	0.150	153
meso-TiWP-30	4.3	0.120	154

Table 4.
Textural properties of the meso-TiWP-x materials derived from nitrogen adsorption/desorption analysis.

of mesoporous titanium tungstosilicate to enrich the metals ions absorption from water was tested by adding aliquots of metal ions solution to a known weight of *meso*-TiWSi-x absorbent. **Figure 13** shows the effect of the *meso*-TiWSi-x loading on the removal efficiency of Cd(II), Hg(II) and Pb(II) ions at pH equals 7 and 25°C. It is observed that the Cd(II) ion uptakes are independent on absorbent loading of *meso*-TiWSi-10 (**Figure 13a**) and the removal efficiency stabilized at around 92%. On the other hand, for Hg(II) ion uptakes gradually increase as the meso-TiWSi-10 absorbent load increases reaching about 92% at 200 mg *meso*-TiWSi-10 loading. However, for Pb(II) ion adsorption at *meso*-TiWSi-10 is inconsistent and unexpectedly shows a decrease in absorption efficiency as the absorbent loading increased. **Figure 13b** shows with the addition of *meso*-TiWSi-20 adsorbent in the range of 50–200 mg, no significant variation in the metal ions uptakes were observed for Hg(II), whereas slight decrease in Cd(II) ions removals was maintained. In contrast, the Pb(II) ions uptakes show a remarkable increase in a number of *meso*-TiWSi-20 adsorbent increases and 80% removal efficiency was achieved at 200 mg

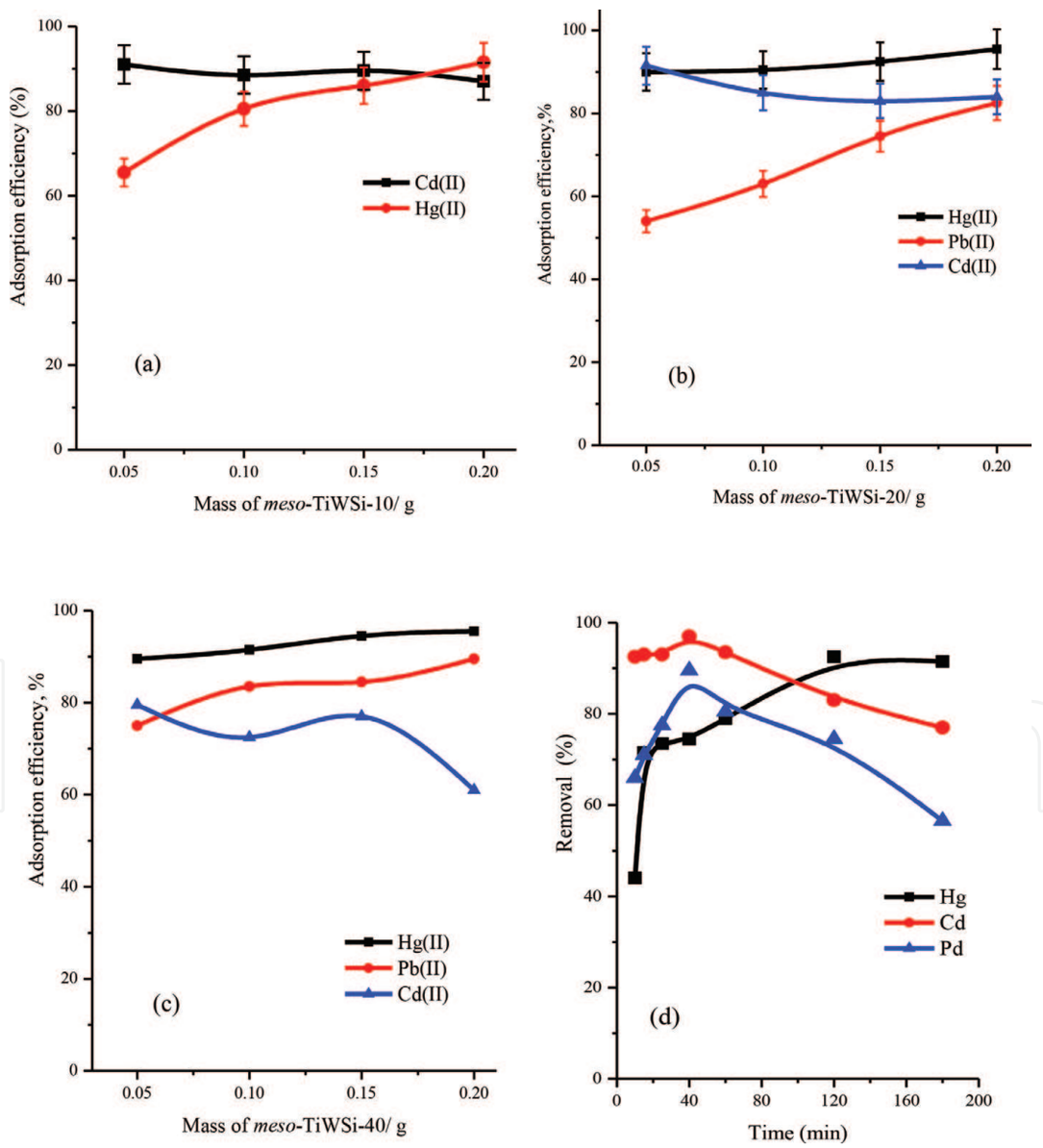

Figure 13.
Effect of the adsorbent dose of (a) meso-TiWSi-10, (b) meso-TiWSi-20, (c) meso-TiWSi-40 on the adsorption of Pb(II), Cd(II) and Hg(II) from aqueous solution at pH of 7, a contact time of 2 hours and a metal ion concentration of 20 ppm, (d) effect of contact time on the adsorption of Pb(II), Cd(II) and Hg(II) from aqueous solution by m-TiWSi-20 at pH of 5, 0.15 g m-TiWSi-20/3 mL solution and a metal ion concentration of 0.2 mg/L.

adsorbent. Effect of *meso*-TiWSi-40 adsorbent dose on the adsorption of Cd(II), Pb(II) and Cd(II) are shown in **Figure 13c**. The removal efficiency of Hg(II) and Pb(II) gradually increases with increasing the adsorbent dose and record about 90 and 85% respectively. This can attribute to the greater availability of the exchangeable sites or surface area at a higher concentration of the adsorbent. While increasing the *meso*-TiWSi-40 adsorbent dose gave rise to a remarkable decrease in adsorption of Cd(II).

Figure 13d shows the effects of agitation time on the removal efficiency of Hg(II), Cd(II) and Pb(II) using 150 mg of *meso*-TiWSi-20 adsorbent at pH = 6. It was noted that the adsorption of Cd(II) and Pb(II) gradually increases with an increase in agitation time and attains an equilibrium adsorption of 95 and 89% respectively within 40 min. Then the removal efficiency gradually decreases at longer agitation time. This result is important as the equilibrium time is a key parameter for economical wastewater treatment applications. On the other hand, the adsorption equilibrium time for Hg(II) takes about 2 hours to reach adsorption efficiency of 90%.

The mesoporous titanium tungstophosphate (*meso*-TiWP) adsorbent was also evaluated for the adsorption of heavy metal ions from water. **Figure 14a** shows the effect of the *meso*-TiWP-15 and *meso*-TiWP-20 adsorbent dose of on the uptakes of Hg(II) ions from water at pH 6. At a fixed Hg(II) ion concentration, it can be observed that the removal % of Hg(II) ion slightly increases with increasing weight of the adsorbents. This is attributed to the high surface area and greater availability of adsorption active sites of *meso*-TiWP-15 and *meso*-TiWP-20 adsorbents. For 95% removal of Hg(II) ion a maximum of 100 mg is required from *meso*-TiWP-15 or *meso*-TiWP-20 adsorbent. **Figure 14b** shows the effect of adsorption time on the removal efficiency of Hg(II), Cd(II) and Pb(II) ions using 150 mg of the *meso*-TiWP-15 absorbent. It is seen that for *meso*-TiWP-15 absorbent exhibited a rapid adsorption for Cd(II) and Pb(II) ions with a removal efficiency reaching about 90% within the first 10 min while it takes about 1.0 hour to achieve 80% for Hg(II) adsorption.

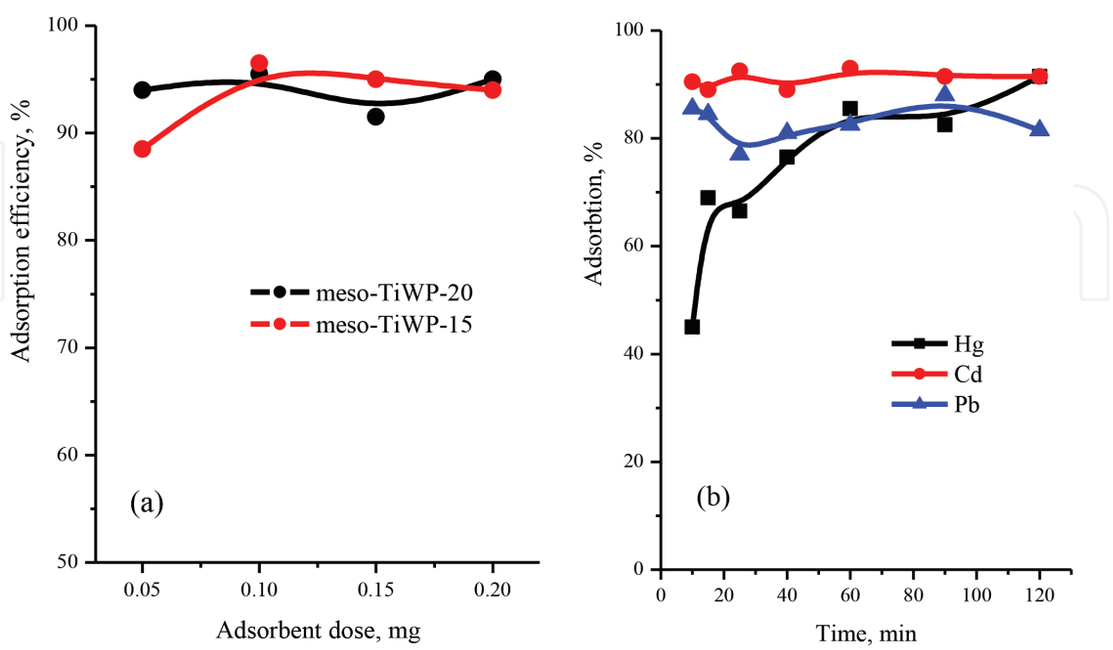

Figure 14.
(a) Effect of the meso-TiWP-15 and a meso-TiWP-20 dose of on the adsorption of Hg(II) from aqueous solution, experimental conditions included a solution pH of 6, a contact time of 2 hours and a metal ion concentration of 20 mg/L, (b) effect of contact time on the adsorption of Pb(II), Cd(II) and Hg(II) from aqueous solution by m-TiWP-15. Experimental conditions included a solution pH of 5, 0.15 g m-TiWP-15/3 mL solution and a metal ion concentration of 0.2 mg/L.

Adsorbent	Cu	Pb	Cd	Hg	Ref.
SBA-15-3-aminopropyl trimethoxy-silane	98.0	99.0	90.0	—	[48]
KIT-6-ethylenediaminetetraacetic acid (EDTA)	99.5	98.0	99.0	—	[49]
SBA-15-ethylenediaminetetraacetic acid (EDTA)	99.0	98	99.5	—	[49]
SBA-15-aminopropyl (SBA/NH_2)	—	96	50	—	[50]
Magnetic MCM-48 mesoporous silica amine (—NH_2)	91	96	90	—	[51]
meso-TiWP-20	95.9	95.5	95.8	—	This work
meso-TiW-20	50	76	—	—	This work
meso-TiWSi-10	—	82	91	92	This work

Table 5.
A comparison of the heavy metal ions removal efficiency of the best performance meso-TWSi-x and meso-TiWP-x materials with some of the modified mesoporous silica-based material reported in the literature.

Finally, **Table 5** shows a comparison of the heavy metal ions removal efficiency of the best performance of our mesoporous titanium tungstophosphate and tungstosilicate materials with some of the modified mesoporous silica-based material widely reported in the literature at similar experimental conditions. Mesoporous *meso*-TiWP-20 showed a good performance for removing Cu^{2+}, Pb^{2+}, and Cd^{2+} in the pH region of 5.0–7.0 which is comparable to the performance, for example, mesoporous silica modified with amine functional group and magnetic iron oxide. This metal ion adsorption enhancement can be apparently attributed to the higher surface area and active sites available to metal ion binding at the surface of *meso*-TiWP and *meso*-TiWSi adsorbents [7].

4. Conclusion

In this work we investigate the synthesis of new bi- and tri-component of mesoporous oxides of titanium tungstate (TiW), titanium tungstosilicate (TiWSi) and titanium tungstophosphate (TiWP) oxides. For the mesoporous titanium tungstosilicate, the silica content was varied between 10, 15, 20, 40 and 60 wt. % using TEOS precursor, while for mesoporous titanium tungstophosphates the ratio of phosphorus was varied as 5, 10, 15, 20 and 30 wt. % by adding PCl_5 into the EISA template mixture of P®123 surfactants, $Ti(OBu)_4$ and WCl_6 precursors. Subject to silica and phosphorus content, the obtained *meso*-TiWSi-x and *meso*-TiWP-x exhibits high surface area, ordered 2D hexagonal mesostructure with orderly channels extended over a large domain. The EISA approach demonstrates a successful synthesis approach for the synthesis of new complex inorganic nanostructured and mesoporous materials for potential application in environmental and catalysis. The produced *meso*-TiW, *meso*-TiWSi, and *meso*-TiWP adsorbents exhibit good adsorbent efficiency for the removal of Pb(II), Cd(II) and Hg(II) ions from water due to the presence of high surface area and accessibility of surface active sites. The adsorption of these metal ions is found to be dependent on contact time and adsorbents dose.

Acknowledgements

This work was funded by The National Plan for Science, Technology, and Innovation (MAARIFAH) King Abdulaziz City for Science and Technology, Kingdom of Saudi Arabia, Award number AT34-203. The authors appreciate Dr. Yuhui Li and Prof. Dongyuan Zhao from Fudan University for their cooperation in the SEM and TEM analysis.

Conflict of interest

There is no any conflict of interest can be declared.

Author details

Mohamed A. Ghanem*, Abdullah M. Al-Mayouf and Mabrook S. Amer
Electrochemical Science Research Chair (ESRC), Chemistry Department, King Saud University, Riyadh, Kingdom of Saudi Arabia

*Address all correspondence to: mghanem@ksu.edu.sa

IntechOpen

© 2019 The Author(s). Licensee IntechOpen. This chapter is distributed under the terms of the Creative Commons Attribution License (http://creativecommons.org/licenses/by/3.0), which permits unrestricted use, distribution, and reproduction in any medium, provided the original work is properly cited. CC BY

References

[1] Hua M, Zhang S, Pan B, Zhang W, Lv L, Zhang Q. Heavy metal removal from water/wastewater by nanosized metal oxides: A review. Journal of Hazardous Materials. 2012;**211-212**:317-331

[2] Fuchs V, Méndez L, Blanco M, Pizzio L. Mesoporous titania directly modified with tungstophosphoric acid: Synthesis, characterization and catalytic evaluation. Applied Catalysis A: General. 2009;**358**:73-78

[3] Wan Y, Yang H, Zhao D. Host-guest chemistry in the synthesis of ordered nonsiliceous Mesoporous materials. Accounts of Chemical Research. 2006;**39**:423

[4] Yang H, Zhao D. Synthesis of replica mesostructures by the nanocasting strategy. Journal of Materials Chemistry. 2005;**15**:1217-1231

[5] Blanco MN, Pizzio LR. Properties of mesoporous tungstosilicic acid/titania composites prepared by sol-gel method. Applied Surface Science. 2010;**256**:3546-3553

[6] Walcarius A. Mesoporous materials and electrochemistry. Chemical Society Reviews. 2013;**42**:4098-4140

[7] Choi J, Ide A, Truong YB, Kyratzis IL, Caruso RA. High surface area mesoporous titanium–zirconium oxide nanofibrous web: A heavy metal ion adsorbent. Journal of Materials Chemistry A. 2013;**1**:5847-5853

[8] Zhang R, Elzatahry AA, Al-Deyabb SS, Zhao D. Mesoporous titania: From synthesis to the application. Nano Today. 2012;**7**:344-366

[9] Collins PJ. Liquid Crystals: Nature's Delicate State of Matter. Princeton: Princeton University Press; 1990

[10] Ghanem MA. Electrochemical synthesis of nanostructured porous materials using liquid crystal and colloidal templates and their magnetic and optical properties [PhD thesis]. University of Southampton; 2002

[11] Attard GS, Glyde JC, Göltner CG. Liquid-crystalline phases as templates for the synthesis of mesoporous silica. Nature. 1995;**378**:366-368

[12] Attard GS, Bartlett PN, Coleman NBR, Elliott JM, Owen JR, Wang JHW. Mesoporous platinum films from lyotropic liquid crystalline phases. Science. 1997;**278**:838-840

[13] Bagshaw SA, Prouzet E, Pinnavaia TJ. Templating of mesoporous molecular sieves by nonionic polyethylene oxide surfactants. Science. 1995;**269**:1242-1244

[14] Kresge CT, Leonowicz ME, Roth WJ, Vartuli JC, Beck JS. Ordered mesoporous molecular sieves synthesized by a liquid-crystal template mechanism. Nature. 1992;**359**:710-712

[15] Martin CR. Nanomaterials: A membrane-based synthetic approach. Science. 1994;**266**:1961-1966

[16] Martin CR. Membrane-based synthesis of nanomaterials. Chemistry of Materials. 1996;**14**:1739-1746

[17] Huo Q, Margolese DI, Stucky GD. Surfactant control of phases in the synthesis of mesoporous silica-based materials. Chemistry of Materials. 1996;**8**(5):1147-1160

[18] Bartlett PN, Baumberg JJ, Birkin PR, Ghanem MA, Netti MC. Highly ordered macroporous gold and platinum films formed by electrochemical deposition through templates assembled from submicron diameter monodisperse polystyrene spheres. Chemistry of Materials. 2002;**14**(5):2199-2208

[19] Xia Y, Mokaya R. Hollow spheres of crystalline porous metal oxides: A generalized synthesis route via nanocasting with mesoporous carbon hollow shells. Journal of Materials Chemistry. 2005;**15**:3126-3131

[20] Wongsakulphasatch S, Kiatkittipong W, Saiswat J, Oonkhanond B, Striolo A, Assabumrungrat S. The adsorption aspect of Cu^{2+} and Zn^{2+} on MCM-41 and SDS-modified MCM-41. Inorganic Chemistry Communications. 2014;**46**:301-304

[21] Da'na E. Adsorption of heavy metals on functionalized-mesoporous silica: A review. Microporous and Mesoporous Materials. 2017;**247**(154):145-157

[22] Lee J-Y, Chen CH, Cheng S, Li HY. Adsorption of Pb(II) and Cu(II) metal ions on functionalized large-pore mesoporous silica. International journal of Environmental Science and Technology. 2016;**13**:65-76

[23] Pérez-Quintanilla D, Sánchez A, Sierra I. Preparation of hybrid organic-inorganic mesoporous silicas applied to mercury removal from aqueous media: Influence of the synthesis route on adsorption capacity and efficiency. Journal of Colloid and Interface Science. 2016;**472**:126-134

[24] Zhu W, Wang J, Wu D, Li X, Luo Y, Han C, et al. Investigating the heavy metal adsorption of mesoporous silica materials prepared by microwave synthesis. Nanoscale Research Letters. 2017;**12**:323

[25] Lin L, Thirumavalavan M, Lee JF. Facile synthesis of thiol-functionalized mesoporous silica-their role for heavy metal removal efficiency. Clean: Soil, Air, Water. 2015;**43**:775-785

[26] Wang C, Chen D, Jiao X. Lyotropic liquid crystal directed synthesis of nanostructured materials. Science and Technology of Advanced Materials. 2009;**10**:23001-23011

[27] Ernst S. Advances in Nanoporous Materials. Vol. 1. Amsterdam, Netherlands: Elsevier; 2009

[28] Yue Y, Gao Z. Synthesis of mesoporous TiO_2 with a crystalline framework. Chemical Communications. 2000;**18**:1755-1756

[29] Boettcher SW, Fan J, Tsung C-K, Shi Q, Stuky G. Harnessing the sol-gel process for the assembly of non-silicate mesostructured oxide materials. Accounts of Chemical Research. 2007;**40**:784-792

[30] Brinker CJ, Lu YF, Sellinger A, Fan HY. Evaporation-induced self-assembly: Nanostructures made easy. Advanced Materials. 1999;**11**(7):579-585

[31] Grosso D, Cagnol F, Soler-Illia GJDA, Crepaldi EL, Amenitsch H, Brunet-Bruneau A, et al. Fundamentals of mesostructuring through evaporation-induced self-assembly. Advanced Functional Materials. 2004;**14**(4):309-322

[32] Zhang Y, Zhao X-C, Wang Y, Zhou L, Zhang J, Wang J, et al. Mesoporous Ti–W oxide: Synthesis, characterization, and performance in selective hydrogenolysis of glycerol. Journal of Materials Chemistry A. 2013;**1**:3724-3732

[33] Miao Z, Song H, Zhao H, Xu L, Chou L. One-pot synthesis of mesoporous ZrPW solid acid catalyst for liquid phase benzylation of anisole. Catalysis Science & Technology. 2014;**4**:838-850

[34] Kuang IL, Hsueh Y-C, Chen H-S, Perng T-P. Mesoporous TiO_2/WO_3 hollow fibers with interior interconnected nanotubes for photocatalytic application. Journal of Materials Chemistry A. 2014;**2**:5387-5393

[35] Amphlet CB. Inorganic Ion Exchangers. Amsterdam: Elsevier; 1964

[36] Clearfield A, Nancollas GH, Blessing RH, Marinsky JA, Marcus Y. Ion Exchanger and Solvent Extraction. Vol. 5. New York: Marcel Dekker; 1973

[37] Clearfeld A. Inorganic ion exchangers with layered structures. Annual Review of Materials Science. 1984;**14**:205-229

[38] Mirajkar SP, Thangaraj A, Shiralkar VP. Sorption properties of titanium silicate molecular sieves. The Journal of Physical Chemistry. 1992;**96**:3073-3079

[39] Tegehall PE. Ion exchange on a titanium phosphate and formation of new crystalline phases by hydrolysis of the ion-exchanged phases. Acta Chemica Scandinavica. 1989;**43**:322-330

[40] Siddiqi ZM, Pathania D. Titanium(IV) tungstosilicate and titanium(IV) tungstophosphate: Two new inorganic ion exchangers. Journal of Chromatography. A. 2003;**987**:147-158

[41] Yavari R, Ahmadi SJ, Huang YD, Khanchi AR, Bagheri G, He JM. Synthesis, characterization and analytical application of a new inorganic cation exchanger-titanium (IV) molybdophosphate. Talanta. 2009;**77**:1179-1184

[42] Bennett WW, Teasdale PR, Panther JG, Welsh DT, Jolley DF. New diffusive gradients in a thin film technique for measuring inorganic arsenic and selenium(IV) using a titanium dioxide based adsorbent. Analytical Chemistry. 2010;**82**:7401-7407

[43] Yang P, Zhao D, Margolese DI, Chmelka BF, Stucky GD. Generalized syntheses of large-pore mesoporous metal oxides with semicrystalline frameworks. Nature. 1998;**396**:152-155

[44] Zhao D, Feng J, Huo Q, Melosh N, Fredrickson GH, Chmelka BF, et al. Triblock copolymer syntheses of mesoporous silica with periodic 50 to 300-angstrom pores. Science. 1998;**279**:548-552

[45] Yuan Q, Liu Y, Li LL, Li ZX, Fang CJ, Duan WT, et al. Highly ordered mesoporous titania-zirconia photocatalyst for applications in degradation of rhodamine-B and hydrogen evolution. Microporous and Mesoporous Materials. 2009;**124**:169

[46] Calleja G, Serrano DP, Sanz R, Pizarro P. Mesostructured SiO_2-doped TiO_2 with enhanced thermal stability prepared by a soft-templating sol-gel route. Microporous and Mesoporous Materials. 2008;**111**:429

[47] Sing KSW, Everett DH, Haul RAW, Moscou L, Pierotti RA, Rouquerol J, et al. Reporting physisorption data for gas/solid systems with special reference to the determination of surface area and porosity. Pure and Applied Chemistry. 1985;**57**:603-619

[48] Da'na E, Sayari A. Adsorption of heavy metals on amine-functionalized SBA-15 prepared by co-condensation: Applications to real water samples. Desalination. 2012;**285**:62-67

[49] Ezzeddine Z, Batonneau-Gener I, Pouilloux Y, Hamad H, Saad Z, Kazpard V. Divalent heavy metals adsorption onto different types of EDTA-modified mesoporous materials: Effectiveness and complexation rate. Microporous and Mesoporous Materials. 2015;**212**:125-136

[50] Hami DM, Yaftian MR, Pilehvari M, Rostamnia S. SBA-15 mesoporous materials decorated with organic ligands: Use as adsorbents for heavy metal ions. Journal of the Iranian Chemical Society. 2015;**12**:561-572. DOI: 10.1007/s13738-014-0513-8

[51] Anbia M, Kargosha K, Khoshbooei S. Heavy metal ions removal from aqueous media by modified magnetic mesoporous silica MCM-48. Chemical Engineering Research and Design. 2015;**93**:779-788

IntechOpen

IntechOpen